J|A|C|S
ARTICLES
Published on Web 07/02/2002

Tripyrrolylphosphine as a Unique Bridging Ligand in the $Rh_6(CO)_{14}(\mu_2\text{-}P(NC_4H_4)_3)$ Cluster: Structure, Bonding, Fluxionality, Thermodynamics, and Kinetics Studies

Claudia Babij,[†] C. Scott Browning,[†] David H. Farrar,[†] Igor O. Koshevoy,[‡] Ivan S. Podkorytov,[§] Anthony J. Poë,*[,†] and Sergey P. Tunik[‡]

Contribution from Lash Miller Chemical Laboratories, University of Toronto, 80 St. George St., Toronto, Ontario, Canada M5S 3H6, Department of Chemistry, St. Petersburg University, Universitetskii pr.2, St. Petersburg, 198904, Russia, and S. V. Lebedev Central Synthetic Rubber Research Institute, Gapsalskaya 1, St. Petersburg, 198035, Russia

Received October 26, 2001

Abstract: Tripyrrolylphosphine reacts with the cluster $Rh_6(CO)_{15}(NCMe)$ to afford the disubstituted $Rh_6(CO)_{14}(\mu_2\text{-}P(NC_4H_4)_3)$ derivative (**2**) via the $Rh_6(CO)_{15}P(NC_4H_4)_3$ intermediate (**1**) with η^1-P coordination. In the solid state, **2** has the phosphine occupying a bridging position where it is bonded to two neighboring Rh atoms in the Rh_6 octahedron through the P-atom and an approximately tetrahedral α-carbon atom of one of the pyrrolyl rings. This can be described by the interaction of an electron pair, associated with a negative charge on one of the canonical forms of the NC_4H_4 ring, with the adjacent Rh center. ^{1}H NMR spectra show that the solid-state structure is retained in solution, but the phosphine is not rigid, and three distinctive dynamic processes are observed. Each of these represents independent hindered rotation of inequivalent pyrrolyl rings about P−N bonds, the ring involved in the interaction with the Rh_6 skeleton displaying the highest activation barrier with $\Delta H^{\ddagger} = 15.8 \pm 0.1$ kcal mol^{-1} and $\Delta S^{\ddagger} = 1.4 \pm 0.3$ cal K^{-1} mol^{-1}. The assignment has been confirmed by ^{1}H TOCSY and EXSY experiments, and a mechanism is proposed. The formation of **2** from **1** is reversible in the presence of CO, which is highly unusual for bridged clusters. The kinetics of the forward and reverse reactions have been studied, and the values of ΔH° and ΔS° for formation of **2** ($+1.3 \pm 0.5$ kcal mol^{-1} and -9 ± 2 cal K^{-1} mol $^{-1}$, respectively) show that the Rh−C bond in the bridge is comparable in strength with the Rh−CO bond it replaces. The intrinsic entropy of **2** is exceptionally unfavorable, overcoming the favorable entropy caused by CO release, and this allows the reversibility of bridge formation. The reactions proceed via a reactive intermediate that may involve agostic bonding of the ring. The reverse reaction has an exceedingly unfavorable activation entropy that emphasizes the unique nature of **2**.

Introduction

Phosphine ligands containing aromatic substituents are versatile and widely used reagents in organometallic chemistry. Involvement of aryl groups attached to the phosphorus atom in coordination to metal centers is an interesting part of their chemistry, a feature which is not as well explored as the primary coordination of the ligands through the phosphorus atom. Secondary interaction of the phosphine substituents with a metal center can result in well-documented orthometalation of phenyl rings[1] or coordination of aryl radicals in η^2-(C═C),[2a−e] η^6-(C_6),[2f−i] and η^2-(C−H)[3] modes. However, to our knowledge, no examples of the secondary coordination of five-membered pyrrolyl phosphine substituents have yet been published. We have found that reaction of tripyrrolylphosphine, $P(NC_4H_4)_3$, with $Rh_6(CO)_{15}(NCMe)$ initially afforded the monosubstituted cluster $Rh_6(CO)_{15}(P(NC_4H_4)_3)$ (**1**), with the usual η^1-ligand coordination mode, but the latter compound spontaneously transforms into the $Rh_6(CO)_{14}(P(NC_4H_4)_3)$ cluster (**2**) with the loss of a CO ligand. Cluster **2** can also be obtained in a one-stage process by reaction of the ligand with the disubstituted acetonitrile cluster, $Rh_6(CO)_{14}(NCMe)_2$. The crystallographic characterization of **2** shows that one NC_4H_4 ring is bonded in a unique fashion, via one α-carbon atom, to a Rh atom next to the originally substituted one. The same structure is maintained in solution, and the dynamic behavior of the ligand has been elucidated by means of 1D ^{1}H VT, 2D ^{1}H TOCSY and EXSY,

* To whom correspondence should be addressed. E-mail: apoe@chem.utoronto.ca.
[†] Lash Miller Chemical Laboratories, University of Toronto.
[‡] Department of Chemistry, St. Petersburg University.
[§] S. V. Lebedev Central Synthetic Rubber Research Institute.

(1) (a) Bennet, M. A.; Dirnberger, T.; Hockless, D. C. R.; Wenger, E.; Willis, A. C. *J. Chem. Soc., Dalton Trans.* **1998**, 271. (b) Bender, M.; Bouaoud, S.-E.; Braunstein, P.; Dusausoy, Y.; Merabet, M.; Raya, J.; Rouag, D. *J. Chem. Soc., Dalton Trans.* **1999**, 735. (c) Deeming, A. J.; Stchedroff, M. *J. Chem. Soc., Dalton Trans.* **1998**, 3819. (d) Waterman, S. M.; Tolhurst, W. A.; Humphrey, M. G.; Skelton, B. W.; White, A. H. *J. Organomet. Chem.* **1996**, *515*, 89. (e) Mirza, H. A.; Vittal, J. J.; Puddephat, R. J. *Can. J. Chem.* **1995**, *73*, 903. (f) Estevan, F.; Lahuerta, P.; Peris, E.; Ubeda, M. A.; Garciagranda, S.; Gomezbeltran, F.; Perezcarreno, E.; Gonzalez, G.; Martinez, M. *Inorg. Chim. Acta* **1994**, *218*, 189.

10.1021/ja012440b CCC: $22.00

Table 1. Bond Lengths [Å] and Angles [deg] for **2**

Rh(10)−Rh(20)	2.7270(9)	P−N(1)	1.691(7)
Rh(10)−Rh(21)	2.7520(9)	N(1)−C(111)	1.393(11)
Rh(10)−Rh(30)	2.7745(9)	N(1)−C(114)	1.385(11)
Rh(10)−Rh(31)	2.7616(9)	C(111)−C(112)	1.363(12)
Rh(10)−P	2.223(2)	C(112)−C(113)	1.445(13)
Rh(10)−C(10)	2.256(9	C(113)−C(114)	1.350(12)
Rh(10)−C(11)	2.137(9)	P−N(2)	1.683(7)
Rh(10)−C(40)	1.895(10)	N(2)−C(121)	1.410(11)
Rh(20)−Rh(21)	2.7783(9)	N(2)−C(124)	1.415(11)
Rh(20)−Rh(30)	2.7285(10)	C(121)−C(122)	1.355(12)
Rh(20)−Rh(40)	2.7036(9)	C(122)−C(123)	1.421(13)
Rh(20)−C(134)	2.310(9)	C(123)−C(124)	1.371(12)
Rh(20)−C(10)	2.124(9)	P−N(3)	1.735(7)
Rh(20)−C(20)	2.109(8)	N(3)−C(131)	1.362(11)
Rh(20)−C(60)	1.876(9)	N(3)−C(134)	1.424(11)
Rh(21)−C(20)	2.222(8)	C(131)−C(132)	1.382(12)
Rh(30)−C(10)	2.186(9)	C(132)−C(133)	1.385(13)
Rh(40)−C(20)	2.242(8)	C(133)−C(134)	1.407(12)
		C(134)−H(134)	0.83(8)

N(3)−P−Rh(10)	110.8(3)	Rh(20)−C(134)−N(3)	108.2(5)
C(131)−N(3)−C(134)	108.1(7)	Rh(20)−C(134)−C(133)	103.9(5)
C(131)−N(3)−P	127.2(6)	Rh(20)−C(134)−H(134)	99(5)
C(134)−N(3)−P	120.6(6)	N(3)−C(134)−C(133)	105.5(8)
N(3)−C(131)−C(132)	109.8(8)	N(3)−C(134)−H(134)	118(6)
C(131)−C(132)−C(133)	107.2(8)	C(133)−C(134)−H(134)	121(7)
C(132)−C(133)−C(134)	109.2(8)	P−Rh(10)−Rh(20)	89.55(6)

and ^{1}H-{^{13}C} HSQC NMR spectroscopy. A kinetic study of the interconversion of **2** and **1** is also reported, together with activation and thermodynamic parameters.

Experimental Results

General. Details of experimental procedures are given as Supporting Information. The clusters and $P(NC_4H_4)_3$ were prepared, purified, and characterized as described elsewhere.[4−6] Reactions were monitored by FTIR spectroscopy,[6] and crystallographic data for the bridged cluster **2** were collected on a Nonius Kappa CCD diffractometer using graphite monochromated Mo Kα radiation ($\lambda = 0.71073$ Å) at 100 K and were analyzed by published methods.[7−10] In the final refinement cycles, the H atoms associated with the pyrrolyl groups were first positioned on geometric grounds and included (as riding atoms) in the structure factor calculation. (H U_{iso} was 20% larger than that for the corresponding C atom.) Subsequently, a unique refinement of H134 was performed as follows (with all other H atoms fixed as above): the C134−H134 bond distance was allowed to refine freely, next the U_{iso} of H134 was refined freely, and, finally, all restraints on H134 were removed, and H134 was refined as a free atom. A correction for secondary extinction was made. Selected bond lengths and angles are given in Table 1, and an ORTEP[9] view of the molecule showing the labeling scheme is shown in Figure 1.

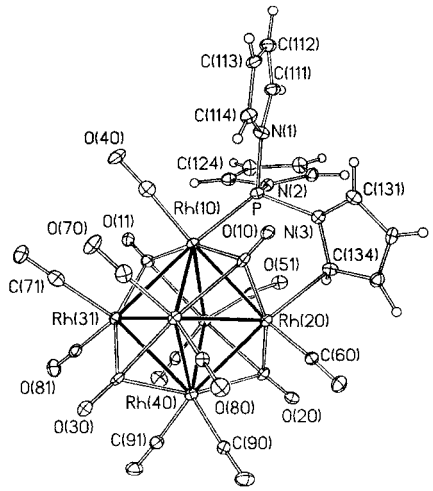

Figure 1. A projection of molecule **2**.

The ^{1}H NMR spectra of $Rh_6(CO)_{14}P(NC_4H_4)_3$ from −50 to +50 °C are illustrated in Figure 2. The ^{1}H TOCSY, ^{1}H-{^{13}C} HSQC, and ^{1}H EXSY are shown in Figures 3−5, respectively. The acquisition parameters common to the three EXSY spectra are given as Supporting Information. The other acquisition parameters are given in the caption to Figure 5.

Kinetics of the forward and reverse reactions, **1** ⇌ **2** under nitrogen and in toluene, were followed by IR and UV−vis monitoring. Because **1** is not very stable, the forward reaction of eq 2 was initiated by the fast reaction in eq 1.

$$Rh_6(CO)_{15}NCMe + P(NC_4H_4)_3 \xrightarrow[-NCMe]{fast} Rh_6(CO)_{15}P(NC_4H_4)_3\ (\mathbf{1}) \quad (1)$$

$$Rh_6(CO)_{15}P(NC_4H_4)_3\ (\mathbf{1}) \overset{slow}{\rightleftharpoons} Rh_6(CO)_{14}P(NC_4H_4)_3\ (\mathbf{2}) + CO \quad (2)$$

The product **1** spontaneously and quantitatively reacts to form **2** (eq 2). In the presence of an excess of free $P(NC_4H_4)_3$, **2** reacts further, and equivalent amounts of $Rh_6(CO)_{15}NCMe$ and $P(NC_4H_4)_3$ were usually used in the kinetic studies so that only **2** is formed. Excellent isosbestic points are observed when monitoring the IR spectra, but trace amounts of $Rh_6(CO)_{16}$ were also detected. Reactions with excess $P(NC_4H_4)_3$ proceed to form what appears to be a mixture of Rh_4 and Rh_2 complexes, but these were not investigated any further. These reactions can also be used to obtain data for the rate of the forward reaction 2 because the reaction of **2** with an excess of $P(NC_4H_4)_3$ is slower than reaction 2.

Solutions for kinetic study of the reaction **2** → **1** were saturated with CO or CO−N_2 mixtures. The FTIR spectra showed that the initial product, **1**, underwent slow reaction to form $Rh_6(CO)_{16}$, although the spectral changes were very clean over a large proportion of the initial reaction. Formation of **1** was incomplete, even under 1 atm of CO and before any appreciable formation of $Rh_6(CO)_{16}$, and the extent of formation of **1** decreased with decreasing partial pressures of CO above the solutions. The solubility of CO in toluene is not available over the whole temperature range used, and it was assumed that the heat of solution is negligible.[11] Corrections for the changing vapor pressure of the solvent were also negligible.[11]

Rate constants were obtained from the time-dependent absorbances at convenient wavenumbers or wavelengths by single or double exponential analysis.

Discussion

Synthesis of $Rh_6(CO)_{14}P(NC_4H_4)_3$ (1). The first stage of reaction between $Rh_6(CO)_{15}NCMe$ and $P(NC_4H_4)_3$ to form **1** is

(2) (a) Shlu, K.-B.; Chou, C.-C.; Wang, S.-L.; Wei, S.-C. *Organometallics* **1990**, *9*, 286. (b) Casas, M. J.; Fornies, J.; Martinez, F.; Rueda, A. J.; Tomas, M. *Inorg. Chem.* **1999**, *38*, 1529. (c) Bradford, C. W.; Nyholm, R. S. *J. Chem. Soc., Chem. Commun.* **1972**, 87. (d) Corrigan, J. F.; Doherty, S.; Taylor, N. J.; Carty, A. J. *J. Am. Chem. Soc.* **1992**, *114*, 7557. (e) Cullen, W. R.; Rettig, S. J.; Zheng, T. C. *Organometallics* **1995**, *14*, 1466. (f) Bowden, J. A.; Colton, R. *Aust. J. Chem.* **1973**, *26*, 43. (g) Roberstson, G. B.; Whimp, P. O. *J. Organomet. Chem.* **1973**, *60*, C11. (h) Hsu, H.-F.; Wilson, S. R.; Shapley, J. R. *Organometallics* **1997**, *16*, 4937. (i) Cullen, W. R.; Rettig, S. J.; Zhang, H. *Organometallics* **1992**, *11*, 1000.
(3) (a) Crabtree, R. H. *Angew. Chem., Int. Ed. Engl.* **1993**, *3216*, 789 and references therein. (b) Brookhart, M.; Green, M. L. H. *J. Organomet. Chem.* **1983**, *250*, 395.
(4) Tunik, S. P.; Vlasov, A. V.; Kryvikh, V. V. *Inorg. Synth.* **1996**, *31*, 239.
(5) Moloy, K. G.; Petersen, J. L. *J. Am. Chem. Soc*. **1995**, *117*, 7707.
(6) Poë, A. J.; Tunik, S. P. *Inorg. Chim. Acta* **1998**, *268*, 189.
(7) Otwinowski, Z.; Minor, W. *Methods Enzymol.* **1977**, *276*, 307.
(8) Siemens Analytical X-ray Instruments Inc. *SHELXTL PC Release 4.1*; Madison, WI, 1990.
(9) Johnson, C. K. *ORTEPII*; Report ornl-5138, Oak Ridge National Laboratory, Oak Ridge, TN, 1976.
(10) *International Tables of Crystallography*; Kynoch Press: Birmingham, 1969; Vol. 4.
(11) Poë, A. J.; Sampson, C. N.; Smith, R. T.; Zheng, Y. *J. Am. Chem. Soc.* **1993**, *115*, 3174 and references therein (particularly 7−9 and 16).

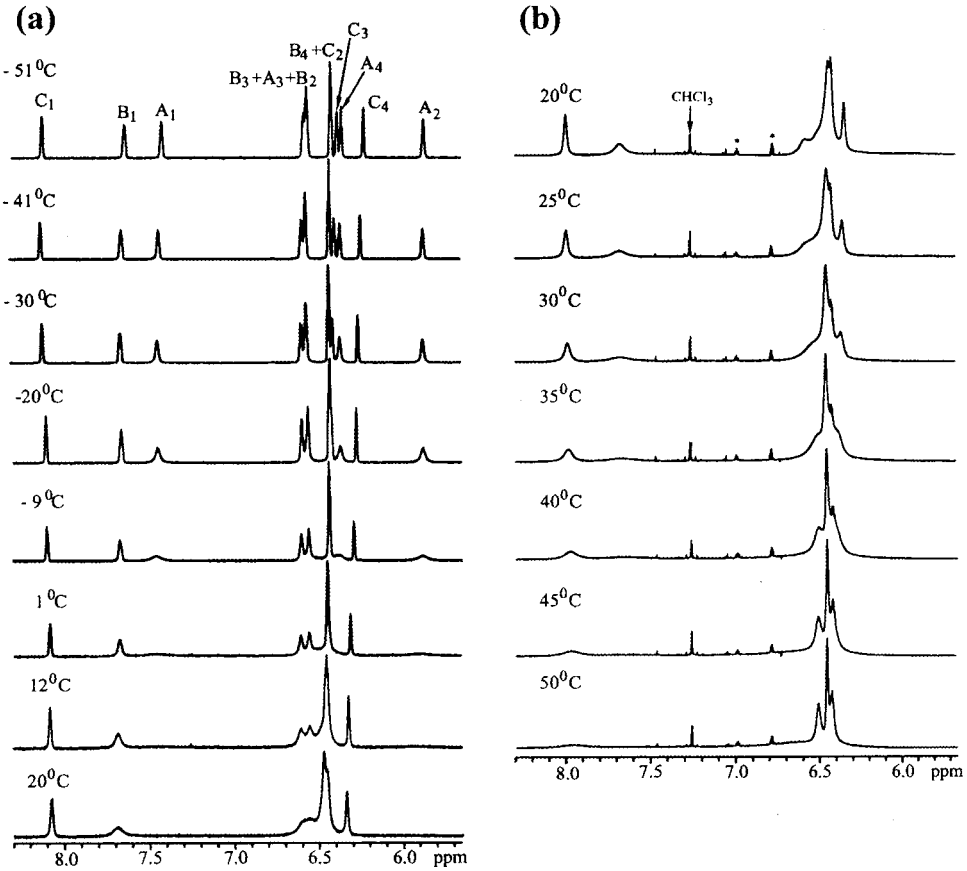

Figure 2. Variable-temperature ^{1}H NMR spectra of **2**: (a) in CD_2Cl_2, (b) in $CDCl_3$. Asterisks denote an impurity.

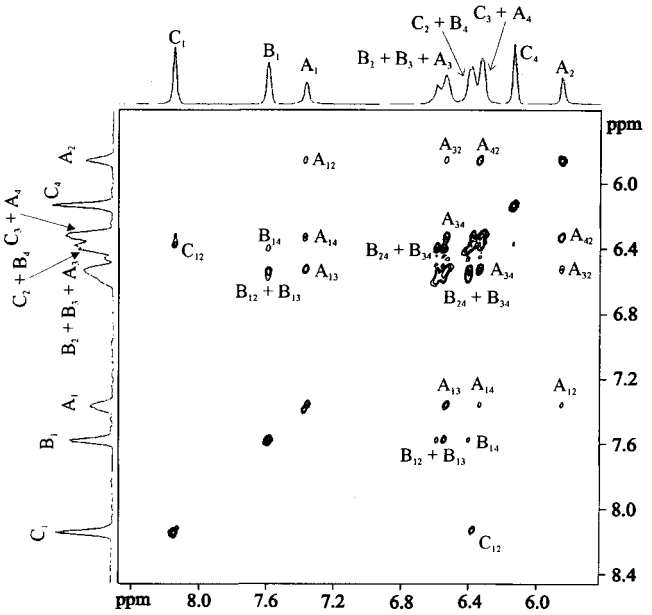

Figure 3. 2D ^{1}H TOCSY spectrum of **2**, CD_2Cl_2, 173 K, 500 MHz, relaxation delay 1.000 s, mixing time 0.080 s.

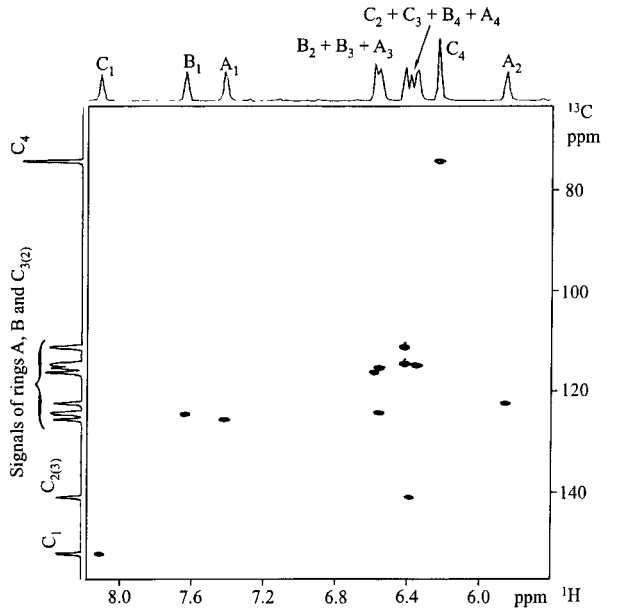

Figure 4. ^{1}H-{^{13}C} HSQC spectrum of **2**, 183 K, relaxation delay 1.000 s.

a typical reaction of the labile acetonitrile derivative with phosphorus donor nucleophiles.[6] These afford simple derivatives with an η^1-coordinated ligand occupying a terminal position on the Rh_6 octahedron, and the IR spectrum of **1** matches well with the spectroscopic patterns of the other monosubstituted derivatives.[12] Also, the ^{31}P spectrum displays a doublet with a typical ^1J(Rh−P) spin−spin coupling constant that clearly points to ligand coordination through the phosphorus atom. However, in contrast to other monosubstituted derivatives,[6,12,13a,b] **1** proved to be spontaneously unstable toward intramolecular displacement of CO to yield **2** on standing in solution for a few hours, or even in the solid state for a few days (eq 2). It was therefore only possible to characterize it by elemental analysis and spectroscopy (IR, ^{31}P NMR, and FAB-MS). Reaction 2 proceeds smoothly to give cluster **2** in quantitative yield provided that no excess of $P(NC_4H_4)_3$ is present and that the CO produced is

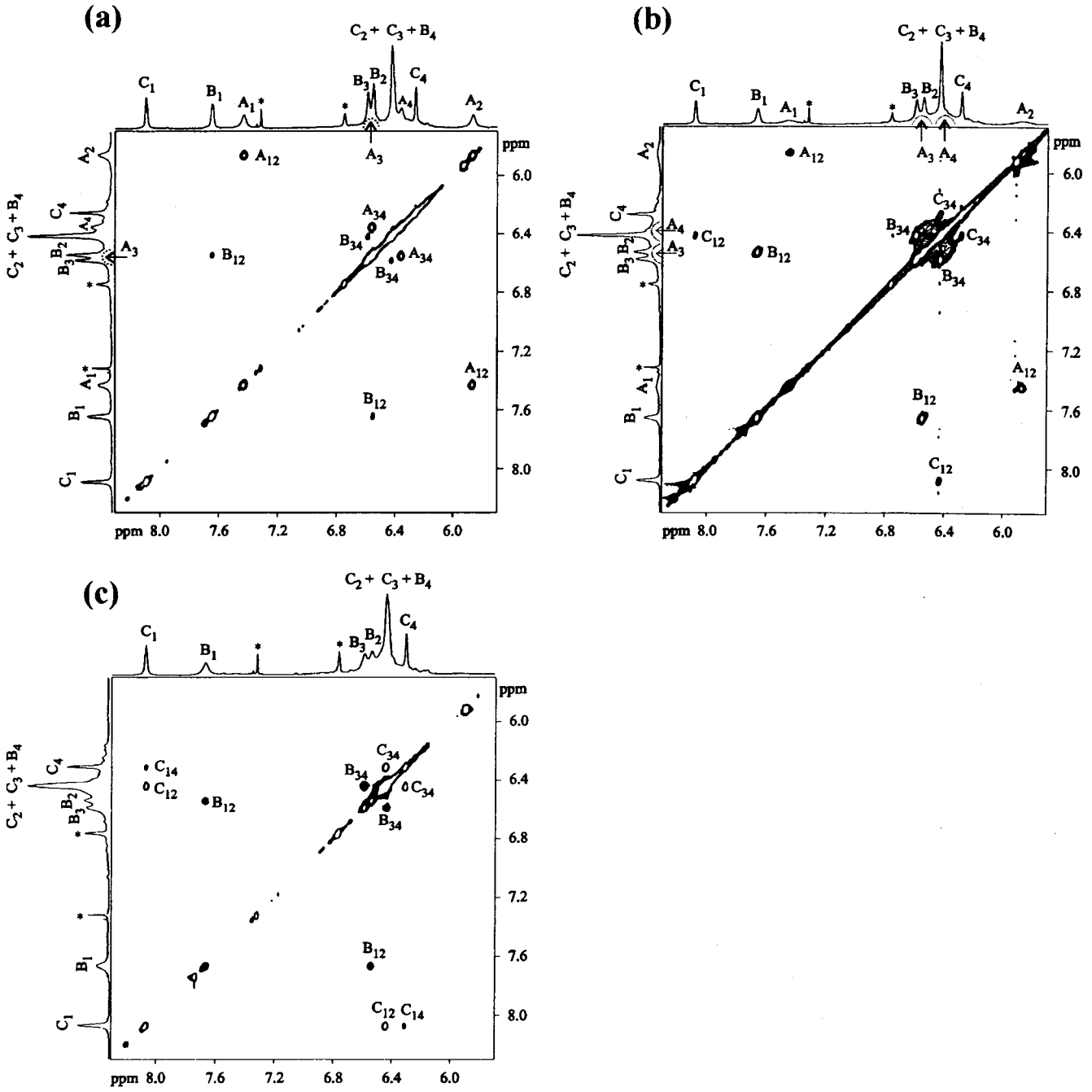

Figure 5. Variable-temperature 2D ^{1}H EXSY spectra of $Rh_6(CO)_{14}P(NC_4H_4)_3$, CD_2Cl_2. (a) $T = 255$ K, relaxation delay $D1 = 4.5$ s, mixing time $D9 = 75$ ms with random variation within $\pm V9 = 25\%$. (b) $T = 270$ K, relaxation delay $D1 = 6$ s, mixing time $D9 = 142$ ms with random variation within $\pm V9 = 25\%$. (c) $T = 285$ K, relaxation delay $D1 = 10$ s, mixing time $D9 = 2.5$ s with random variation within $\pm V9 = 10\%$.

continuously removed by bubbling with nitrogen. Monitoring these reactions using ^{31}P NMR and IR spectroscopy, and chromatography of the product solutions, confirmed that conversion of **1** into cluster **2** occurs quite cleanly, but with the formation of small amounts of $Rh_6(CO)_{16}$ as a byproduct if the CO is not removed. The process is reversible, and saturation of the chloroform solution containing **2** with CO results in reformation of **1**, to a degree that depends on the CO concentration. The acetonitrile derivative, $Rh_6(CO)_{14}(NCMe)_2$, instantly affords **2** by reaction with 1 equiv of $P(NC_4H_4)_3$ (eq 3) and provides another route for the synthesis of **2**.

$$Rh_6(CO)_{14}(NCMe)_2 + P(NC_4H_4)_3 \xrightarrow[-2NCMe]{\text{fast}} Rh_6(CO)_{14}P(NC_4H_4)_3\,(\mathbf{2}) \quad (3)$$

$Rh_6(CO)_{14}P(NC_4H_4)_3$: Structure and Bonding. The $P(NC_4H_4)_3$ ligand in **2** shows itself to be capable of taking part in a form of bridging that is totally novel, involving as it does direct bonding between the second bridged Rh atom and an α-carbon in one of the NC_4H_4 rings. This is shown by the

(12) Farrar, D. H.; Grachova, E. V.; Lough, A.; Patirana, C.; Poë, A. J.; Tunik, S. P. *J. Chem. Soc., Dalton Trans.* **2001**, 2015.
(13) (a) Clucas, J. A.; Harding, M. M.; Maginn, S. J. *J. Chem. Soc., Chem. Commun.* **1988**, 185. (b) Tunik, S. P.; Vlasov, A. V.; Gorshkov, N. I.; Starova, G. L.; Nikol'skii, A. B.; Rybinskaya, M. I.; Batzanov, A. S.; Struchkov, Yu. T. *J. Organomet. Chem.* **1992**, *433*, 189. (c) Pomogailo, S. I.; Chuev, I. I.; Dzhardimalieva, G. I.; Yarmolenko, A. V.; Makhaev, V. D.; Aldoshin, S. M.; Pomogailo, A. D. *Russ. Chem. Bull.* **1999**, *48*, 1174.

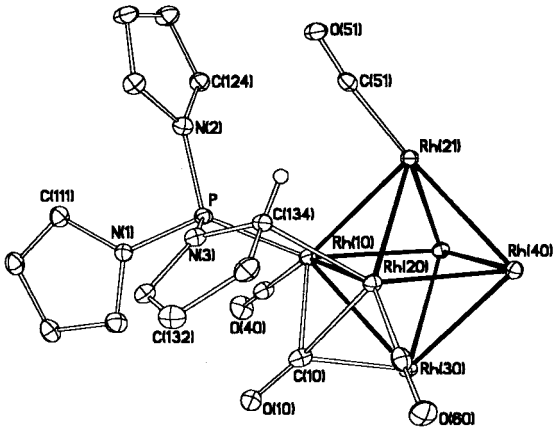

Figure 6. Structure of relevant parts of **2**. Only CO ligands in the neighborhood of the bridging ring are shown.

molecular structure of **2** shown in Figure 1 and by the bond lengths and angles given in Table 1, where the atom numbering follows the convention used previously.[12] The molecule consists of an $\{Rh_6(CO)_{14}\}$ unit, the structure of which is very similar to those found in analogous $Rh_6(CO)_{14}(LL)$ clusters (LL = dppm, dppe).[13a,b] The central rhodium octahedron and four triply bridging CO ligands comprise the same $Rh_6(\mu_3\text{-}CO)_4$ fragment that is found in the parent $Rh_6(CO)_{16}$ complex.[12,14] Of the 12 terminal sites, two at each rhodium atom, 10 are occupied by carbonyl groups, and the bidentate ligand takes up two adjacent positions on an edge of the rhodium octahedron.

In the dppm and dppe substituted clusters, these ligands supply four electrons to compensate for the two displaced carbonyl ligands, thereby maintaining the stable 86 electron configuration of the octahedral cluster core that is typical of $Rh_6(CO)_{16}$ and its substituted derivatives.[4,6,12,13] The spontaneous nature of the transformation of **1** into **2**, and the coordination of the $P(NC_4H_4)_3$ ligand in the bidentate mode, is the first example of a pyrrolyl ring displacing a CO ligand and becoming bonded to a neighboring metal center to form a cluster that is stable enough for its 86 electron configuration to be strongly implied. The ring is therefore presumably able to serve as a two-electron donor.

Because the $\{Rh_6(CO)_{14}\}$ fragment is so little affected by coordination of the $P(NC_4H_4)_3$ ligand, we focus on the dimensions of the $P(NC_4H_4)$ moiety that bridges the Rh(10)−Rh(20) bond as illustrated in Figures 6 and 7.

The geometrical constraints, caused by the bridging mode of the ligand's coordination, tilt the Rh(10)−P bond toward the Rh(20) atom and make the P−Rh(10)−Rh(20) angle (89.55(6)°) somewhat less than the values found for dppm and dppe derivatives (95° and 103°, respectively).[13a,b] As an additional means of providing an effective contact between the Rh(20) atom and the N(3)−pyrrolyl ring, the P−N(3) bond of the coordinated pyrrolyl fragment is displaced from the ring plane by 16.6° as compared with the 3.9° and 8.2° found for noncoordinated N(1) and N(2) rings, respectively.

Another distortion of significance is the displacement of H(134) from the plane of the N(3) pyrrolyl ring, and this results in the geometry around C(134) becoming approximately tetrahedral. Thus, the angles H(134)−C(134)−Rh(20), H(134)−C(134)−C(133), and H(134)−C(134)−N(3) are 99(5)°, 121(7)°, and 118(6)°, respectively, while the Rh(20)−C(134)−C(133), C(133)−C(134)−N(3), and Rh(20)−C(134)−N(3) angles are 103.9(6)°, 105.5(8)°, and 108.2(5)°, respectively. The same conclusion regarding the geometry around C(134) is suggested by the resonance of the C(134) carbon nucleus. As is usually found for sp^2 to sp^3 rearrangements, this resonance is shifted more than 40 ppm to high field as compared with the main group of pyrrolyl carbon resonances (see Figure 4). No other resonances in the ^{13}C dimension are high field shifted with respect to the main group of resonances, and this clearly demonstrates again the unique nature of the C(134) carbon in the cluster structure.

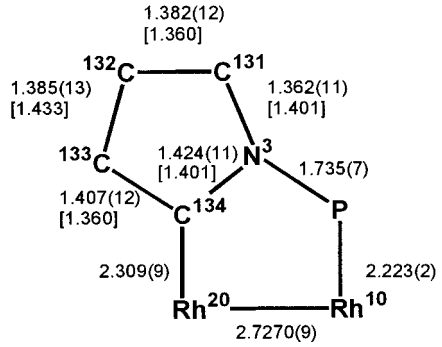

Figure 7. Dimensions of bridging region of **2**. Numbers in brackets are averages of the corresponding bond distances in rings A and B.

As for the interatomic distances shown in Figure 7, the P−Rh(10) distance, 2.223(2**)** Å, is the shortest one in the series of $Rh_6(CO)_{16}$ derivatives containing mono- and bidentate phosphines.[12,13] Thus, the Rh−P distance in $Rh_6(CO)_{15}P(OPh)_3$ is 2.2511(8) Å, and that in $Rh_6(CO)_{15}P(n\text{-}Bu)_3$ is 2.344(2) Å.[12] This shortness of the $Rh-P(NC_4H_4)_3$ bond is in line with an exceptionally low net donor ability of $P(NC_4H_4)_3$ as evidenced by its very large χ value[15] and the related high contribution of π-back-donation in the Rh−P bond.

The other dimensions in Figure 7 provide a comparison between the interatomic distances in the bridging and nonbridging NC_4H_4 moieties. These differences are well described in terms of the very simple model, represented by the three major canonical forms **I**, **II**, and **II′** for the NC_4H_4 ring, shown below.

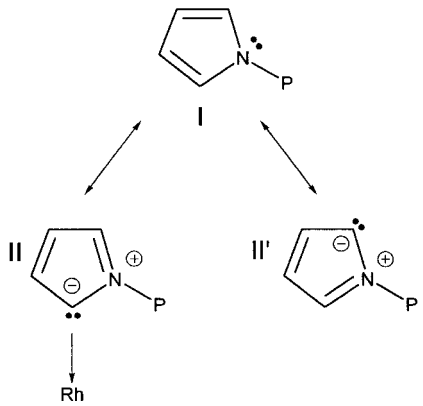

The bonding between the NC_4H_4 ring and Rh(20) can be ascribed largely to the canonical form **II** in the valence bond

(14) Corey, E. R.; Dahl, L. F.; Beck, W. *J. Am. Chem. Soc.* **1963**, *85*, 1202.

(15) Fernandez, A. J.; Reyes, C.; Lee, T. Y.; Prock, A.; Giering, W. P.; Haar, C. M.; Nolan, S. P. *J. Chem. Soc., Perkin Trans. 2* **2000**, 1349. Seron, S.; Nolan, S. P. *Organometallics* **1996**, *15*, 4301. Moloy, K. G.; Peterson, J. L. *J. Am. Chem. Soc.* **1995**, *117*, 7696.

resonance form of the ring. This form has an electron pair on an α-carbon atom of the ring that enables the ring to donate a pair of electrons to Rh(20). Although the other canonical form **II′** also has a pair of electrons on an α-carbon atom, **II** and **II′** cannot both donate their electron pairs to Rh(20) at the same time. This means that, as compared with the free, nonbridging, NC_4H_4 rings attached to the same P atom, the contribution of resonance form **II** will be enhanced, and those of **I** and **II′** will be diminished.

This has the main consequence that the C(134)−Rh(20) distance will be vastly decreased and should approach that of a C−Rh single bond. In fact, the C(134)−Rh(20) distance of 2.310(9) Å compares with the Rh−C distances of 2.06(2) and 1.96(2) Å in $Rh_6(CO)_{15}COEt^-$ and $Rh_6(CO)_{15}COOMe^-$, respectively,[12] and Rh−CH_3 bonds as long as 2.338 Å have been observed.[16] Further, the bond distances in the bridging ring, as compared with the averages of the corresponding distances in the nonbridging rings, are all consistent with the different contributions of the various canonical forms. Thus, the C(131)−C(132) and C(133)−C(134) bonds are lengthened (by ∼0.02 and 0.05 Å, respectively) as expected from the decreased contribution of **I**, and the C(132)−C(133) bond is shortened (by ∼0.05 Å) as expected from the increased contribution of **II**. The C(134)−N(3) bond is lengthened (by ∼0.02 Å), and the C(131)−N(3) bond is shortened (by ∼ 0.04 Å), in accord with the greater importance of **II** as compared with **II′**. Thus, this very simple model is successful in representing the main bond angle and bond length features of this unique molecule. It takes into account the well-documented mobility of the π-electron lone pair on the nitrogen atom in pyrrolyl compounds, and it maintains the 86 electron count of the cluster through the two-electron C(134)−Rh(20) bond.

Other possible sources of a donor pair of electrons can be considered. Double bonds in aromatic rings attached to P-donor atoms are known to be able to coordinate in a bridging manner not unlike the bridging observed here.[2a,b] However, in these cases, the distances between the neighboring metal atom and the two donor C atoms are only slightly different, and the same applies to the bridging CH═CH_2 group in $Rh_6(CO)_{14}(\mu_2,\eta^1{:}\eta^2$-$Ph_2PCH_2CH{=}CH_2)$, where the difference in the Rh−C bond lengths is only 0.05 Å.[13c] The near-symmetrical nature of these coordinated C═C bonds is far from what is observed and discussed above for the $Rh_6(CO)_{14}(\mu_2$-$P(NC_4H_4)_3)$ cluster, where the Rh(20)−C(133) distance of 2.98 Å is over 0.6 Å longer than the Rh(20)−C(134) distance and comparable to the Rh(20)−N(3) nonbonding distance of 3.07 Å. Although the C(133)−C(134) "double bond" in the N(3) ring is elongated by ca. 0.05 Å upon coordination, this can also be explained perfectly well by the simple model described above.

This model also differs significantly from any of the other known modes of bonding that involve organic groups attached to P-donor atoms. Orthometalation would involve formation of a single metal to carbon bond, but this would also require transfer of a hydrogen atom onto the metal core.[1] However, the structural and spectroscopic data obtained clearly show that this is not the case for **2**. In particular, special attention was paid to refinement of the H(134) hydrogen atom which has been unambiguously shown to be displaced on the far side of the pyrrolyl ring from Rh(20). Moreover, all 12 proton resonances appear individually in the 8.2−5.8 ppm interval of the low-temperature limit ^{1}H NMR spectrum, far away from the typical hydride region of −2 to −50 ppm.[17]

Another opportunity for the cluster core to obtain a pair of electrons from the coordinated pyrrolyl ring might be through the agostic interaction[3] of a C−H bond with the unsaturated metal center. However, the potentially agostic Rh(20)−C(134)−H(134) triangle displays structural and spectroscopic characteristics which do not allow this description of the bonding. For example, the displacement of H(134) out of the pyrrolyl ring plane in the direction *away from* the Rh(20) atom is inconsistent with the basic idea of agostic interaction of a C−H bond with a metal center. An agostic interaction would also result in distortion of the angles in the M−C−H triangle so as to allow effective overlapping of the C−H bonding orbital with the empty acceptor orbital on the metal, and this is not what is observed. Moreover, as was pointed out above, the signals in the ^{1}H NMR spectrum display neither the substantial high field shift nor the Rh−H coupling typical of hydrogen atoms involved in agostic bonding. These facts show that the hypothesis of agostic interaction of the pyrrolyl ring with the Rh(20) atom is not tenable.

NMR Spectra. Other NMR spectroscopic data obtained for **2** are in agreement with the structural evidence described above. The ^{1}H NMR spectra in Figure 2 show that the molecule is stereochemically nonrigid at room temperature but becomes static at temperatures below ca. −40 °C as shown by the 12 resonances of the pyrrolyl protons in the range 8.2−5.8 ppm. This correlates well with the completely asymmetrical structure of coordinated $P(NC_4H_4)_3$ found in the solid state. The signals in Figure 2a were assigned using a combination of various spectroscopic techniques as shown in Figures 3−5.

Correlations observed in the TOCSY experiment allow for the dividing of the signals in the 1D spectrum into three groups corresponding to certain pyrrolyl fragments. Inside these groups, the signals denoted A_i, B_j, C_k clearly display the cross-peaks which correspond to the spin−spin couplings in the corresponding pyrrolyl ring. It has to be pointed out that the protons from the C group do not display all possible correlations, and this distinguishes this group from the A and B type protons. Moreover, the absence of some correlations distinguishes the proton couplings in this ring from those in A and B and probably points to electronic density withdrawal from the C ring. This can be ascribed to the effect of coordination and allows further assignment of the C group signals to the N(3) pyrrolyl ring. The correlations observed in Figure 4 for the C group of proton signals reveal that the corresponding ^{13}C resonances appear at 152.0, 140.4, 110.0, and 72.5 ppm. Three of these signals are substantially high- or low-shifted as compared with the other carbon resonances that appear in quite a narrow interval between 124 and 110 ppm. This emphasizes the specific nature of the corresponding pyrrolyl ring and reinforces the assignment of the C group of resonances to the nuclei in the coordinated ring.

The variable-temperature ^{1}H NMR spectra in Figure 2 also illustrate the different behavior of the A, B, and C group protons. As the temperature is raised from the low-temperature limit, each particular group of resonances starts to broaden in the

(16) Herrman, W. A.; Plank, J.; Ziegler, M. L. *J. Am. Chem. Soc.* **1981**, *103*, 63.

(17) Iggo, J. A. *NMR Spectroscopy in Inorganic Chemistry*; Oxford University Press: New York, 1999; p 49.

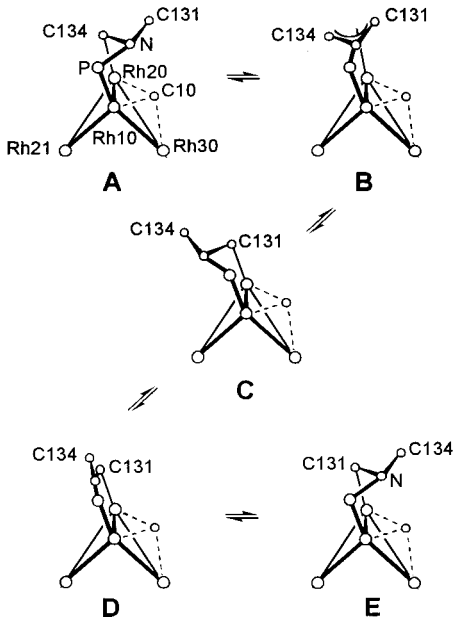

Figure 8. Schematic indication of essential atomic movements that are proposed to accompany the interchange of atoms C(134) and C(131) and their attached hydrogen atoms. (The species **A**−**C** should not be confused with the nomenclature for the pyrrolyl *rings* A−C used in the text.)

following order: first A, then B, and last C. The spectra in Figure 5, recorded at various temperatures, clearly show that the dynamic behavior observed for the protons of the A and B groups is really localized inside these groups and consists of pairwise exchanges of the corresponding protons without cross mixing between two pairs. The most probable dynamic process responsible for the exchanges observed in the 1D VT and 2D ^{1}H EXSY spectra is a hindered rotation of the pyrrolyl moieties about the P−N bond. It is well known that P−N bonds often appear not to be simple single bonds,[18] and the multiple nature of the P−N bonds is manifested in the hindered rotation of the A and B pyrrolyl rings observed in the low-temperature ^{1}H NMR spectra.

The resonances in group C, which have been assigned to the coordinated pyrrolyl ring, do not display appreciable broadening until room temperature. The substantially higher activation barrier for the dynamic process that this fragment is undergoing must be associated with its bonding to the cluster skeleton. The longer N(3)−P bond in the coordinated pyrrolyl ring would indicate less double bonding and more facile rotation in contrast to what is observed.

In the ^{1}H EXSY spectrum recorded at 285 K, one can observe two usual (C_{12} and C_{34}) pairwise correlations that correspond to rotation of the pyrrolyl fragment about the P−N bond. It is significant that, in the temperature range studied, the cluster **2** does not display any exchange between pyrrolyl rings of the ligand. The N(3)−pyrrolyl ring must, therefore, maintain a certain degree of bonding to Rh(20) in the process of rotation about P−N(3). This ensures that the phosphine ligand is never free to rotate about the Rh(10)−P bond and prevents interchange of the N(1), N(2), and N(3) rings.

This basic feature can be accounted for by the sequence of hypothetical but simple atomic movements indicated in Figure 8, where only the essential atoms are included. Structure **A** is similar to that in Figure 6 but looking down slightly along the Rh(10)−Rh(20) bond. Ring C is indicated only by the moiety C(134)−N−C(131). The first step, **A** → **B**, involves conversion, by slippage, of the Rh(20)−C(134) bond until it is replaced by an η^x interaction, where x is probably 5 as suggested by a model of the structure. Continued movement of the C(134)−N−C(131) moiety to the left leads to **C** in which the C(131) is now bound to Rh(20). **C** is the unstable isomer of **A** in which the N atom points toward a *nonbridged* face of the Rh_6 octahedron. Formation of the stable structure **E** can now be accomplished by the movement from right to left of the N atom, the structure passing through **D** which has an essentially planar cyclic Rh(10)−P−N−C(131)−Rh(20) moiety. The hydrogen atoms attached to the C(134) and C(131) atoms remain exo to the ring throughout this whole transformation. Implicit in the reversibility of the steps in the scheme is the possibility of a sequence equivalent to going from **E** through **D**, **C**, and **B** to **A**. There is no way of differentiating these two possibilities, and the rate is determined in either case by the highest free energy barrier to be crossed, irrespective of where it occurs in the sequence.

Table 2. Activation and Thermodynamic Parameters from Eyring or van't Hoff Analyses Based on the Temperature Dependence of Appropriate Rate Constants or Their Combinations

rate constants[a]	ΔH, kcal mol^{-1} [b]	ΔS, cal K^{-1} mol^{-1} [b]	$\sigma(k_{obs})$, %[c]
k_{-co}	23.1 (3)	4.6 (9)	7.0
k_{-c}	5.4 (3)	−51 (1)	3.0
k_{+co}/k_{+c}	16.5 (5)	64 (2)	4.3
$k_{-c}k_{+co}/k_{+c}$[d]	21.8 (8)	13 (3)	7.2
$k_{-c}k_{+co}/k_{+c}$[e]	23 (2)	18 (7)	18.4
$k_{-c}k_{+co}/k_{+c}k_{-co}$	−1.3 (5)	8 (2)	4.3
Δf_T[f]	15.8 (1)	1.2 (5)	

[a] Rate constants, or rate constant combinations, as defined in eqs 5−7. [b] Standard errors of last significant figures are given in parentheses. [c] Standard deviation of individual rate constants, their combinations, or the equilibrium constants as derived from the Eyring or van't Hoff analyses. [d] Obtained from the combination of k_{-c} and k_{+co}/k_{+c}. [e] Obtained from initial slopes of k_{obs} versus [CO] plots as described in the text. [f] Line width at half-height data for ring C (see eq 5).

The temperature-dependent line widths of the band at 8.07 ppm assigned to this scrambling process allow for the derivation of the rate constants by use of eq 4.[19]

$$k_{sc} = \pi(\Delta f_T - \Delta f_{T0}) \quad (4)$$

Here Δf_T is the bandwidth at a given temperature, T, and Δf_{T0} is the bandwidth at the low-temperature limit. Equation 4 is equivalent to eq 5 where E_a is the Arrhenius activation energy,

$$\Delta f_T = (1/\pi)Ae^{-E_a/RT} + \Delta f_{T0} \quad (5)$$

and A is the "preexponential factor". An unweighted analysis[20] of the exponential decrease of Δf_T with increasing $1/T$ leads to values of Δf_{T0}, A, and E_a from which the Eyring activation parameters shown in Table 2 can be calculated. The fit to eq 5 is excellent, the estimated standard deviation in Δf_T being ±1.3

(18) Barton, D.; Ollis, W. D. *Comprehensive Organic Chemistry*; Pergamon Press: Elmsford, NY, 1979; Vol. 2, Chapter 10.6.

(19) Ernst, R. R.; Bodenhausen, G.; Wokaun, A. *Principles of Nuclear Magnetic Resonance in One and Two Dimensions*; Clarendon Press: Oxford, 1987.

(20) Values of rate constants for a particular reaction are usually taken to have the same percentage uncertainty irrespective of temperature. (This is implicit in all Eyring analyses where the ln(k/T) values are weighted equally). However, a constant percent uncertainty in Δf_T (e.g., 10%, or 8 Hz, at 48 °C) would be only 0.6 Hz at 7 °C, and, conversely, a reasonable 1 Hz (15%) uncertainty at 7 °C would be 12 Hz at 48 °C. In practice, this makes little difference to the parameters obtained; the standard deviation of Δf_T, with a constant percent uncertainty, is only ±4%, although the activation parameters are less precise.

Hz. This incorporates any random errors in both Δf_T and $1/T$ and is quite objective, relying only on the fit of the data to eq 5. Systematic errors, in the temperature measurements, for example, might affect the activation parameters, but it would require an error of 2.5 °C over the 40 °C temperature range to produce a 1 kcal mol^{-1} uncertainty in the activation enthalpy. Line broadening data associated with rotation of ring B were also obtained from −5 to +40 °C and led to the values $\Delta H_B^{\ddagger} = 11.1 \pm 0.2$ kcal mol^{-1} and $\Delta S_B^{\ddagger} = -11.6 \pm 0.6$ cal K^{-1} mol^{-1} ($\sigma(\Delta f_T) = \pm 2.0$ Hz). Much less complete data from −5 to +10 °C for line broadening associated with ring A led to the approximate values $\Delta H_A^{\ddagger} = 13$ kcal mol^{-1} and $\Delta S_A^{\ddagger} = -1$ cal K^{-1} mol^{-1} ($\sigma(\Delta f_T) = \pm 7$ Hz). The greater rates of rotation of the two nonbridging NC_4H_4 rings are evidently because of lower enthalpic barriers offset, for ring B, by a less favorable entropic barrier.

The two C_{12} and C_{34} pairwise exchanges (Figure 5) that correspond to rotation of the pyrrolyl fragment about the P−N(3) bond are similar to those observed in A and B pyrrolyl rings, but there is also a weak C_{14} cross-peak. The correlation points to a "nonrotational" exchange, which is evidently related to the migration of the protons across a C═C double bond, a process that was not observed for noncoordinated A and B pyrrolyl rings. As was mentioned above, the C_4 resonance can be reliably assigned to the proton attached to the C(134) carbon, which in turn is bonded to Rh(20). Thus, the dynamics responsible for the C_{14} cross-peak are related to the migration of a proton between two adjacent (C(134) and C(133)) carbon atoms, one of which is coordinated to the rhodium center. It is not clear how this process might be related, if it is at all, to the other scrambling processes, or if this is a distinct and additional process.

Kinetics and Thermodynamics. The kinetic and equilibrium studies of the reversible loss of CO shown in eq 2 provide good quantitative evidence for the strength of this novel type of bonding of an aromatic fragment to an empty coordination site on a metal cluster.

The forward reaction was monitored by time-dependent IR and UV−vis spectroscopy at different wavenumbers or wavelengths and always went to completion. The reverse reaction did not go to completion, even under an atmosphere of pure CO, and its kinetics were studied under atmospheres of CO or CO−N_2 mixtures. The changes of absorbance decrease with decreasing [CO], and the spectroscopic observation of increasing amounts of unreacted **2** showed that an equilibrium mixture of reactants and product was being approached. The forward reaction was not studied under atmospheres of CO because of the competing and complicating reaction to form $Rh_6(CO)_{16}$. Small amounts of this product were seen even when the reaction was carried out under nitrogen, and presumably this arises from the release of CO during the reaction. In obtaining rate constants for these and the reverse reactions from the absorbance changes, allowance for various overlapping reactions was made when necessary by use of double exponential analysis. The agreement between the constants obtained by the different spectroscopic techniques and the different energies monitored was excellent, despite the various complications.

The rate data can be considered in terms of the sequence of reactions shown in eqs 6 and 7 where **Int** represents a steady-state intermediate. The corresponding rate equation

$$Rh_6(CO)_{15}P(NC_4H_4)_3 \underset{k_{+co}}{\overset{k_{-co}}{\rightleftharpoons}} \mathbf{Int} + CO \tag{6}$$

$$\mathbf{Int} \underset{k_{-c}}{\overset{k_{+c}}{\rightleftharpoons}} Rh_6(CO)_{14}(\mu\text{-}P(NC_4H_4)_3) \tag{7}$$

$$k_{obs} = \{k_{-co} + k_{-c}(k_{+co}/k_{+c})[CO]\}/\{1 + (k_{+co}/k_{+c})[CO]\} \tag{8}$$

is given in eq 8 where k_{+c} and k_{-c} represent the respective rate constants for making and breaking the bond between the Rh atom and the α-carbon atom in the bridging $N(C_4H_4)_3$ ring. Values of k_{-co} are obtained directly from the values of k_{obs} for the forward reaction in eq 6, those reactions being carried out under N_2, and activation parameters are given in Table 2. Values for the other derivable kinetic parameters, k_{-c} and k_{+co}/k_{+c}, have to be obtained from values of k_{obs} obtained for the reverse reaction, **2** → **1**, which are dependent on [CO]. Because we can make use of the calculated values of k_{-co}, obtained from the Eyring analysis, there are only two independent remaining unknowns to be calculated at each temperature, viz., $k_{-c}(k_{+co}/k_{+c})$ and (k_{+co}/k_{+c}). Equation 8 can usefully be rearranged to eq 9 where the two independent unknowns are k_{-c} and k_{+co}/k_{+c}. Appropriately chosen values of k_{-c} at each temperature should give linear plots of $(k_{obs} - k_{-co})/(k_{-c} - k_{obs})$ versus [CO] that go through the origin, and these values of k_{-c} should also give good fits to an Eyring plot. Initial values of k_{-c} were "guestimated" by extrapolation of k_{obs} versus [CO] plots, and these were refined by fitting them to Eyring plots. The k_{-c} values taken from the Eyring analysis were further refined until good linear plots of $(k_{obs} - k_{-co})/(k_{-c} - k_{obs})$ versus [CO] were obtained. This method gives precise values of both k_{-c} and k_{+co}/k_{+c} because choosing incorrect values of k_{-c} leads to very nonlinear plots. Not only are these plots satisfactorily linear, but the Eyring analyses, based on the same k_{-c} and k_{+co}/k_{+c} values, are also very good as shown by the activation parameters given in Table 2.[21] Combination of the rate constants k_{-co}, k_{-c}, and k_{+c}/k_{+co} obtained from the corresponding Eyring plots provides values for $K = k_{-co}k_{+c}/k_{+co}k_{-c}$ so that values of $\Delta H°$ and $\Delta S°$ (Table 2) can be obtained from a van't Hoff analysis. Use of these constants also enables values of k_{obs} to be calculated for each value of [CO] at each temperature. The overall fit of the data can be assessed from the value of $\sigma(k_{obs}) = 100[\sum\{(k_{obs} - k_{calc})/k_{calc}\}^2/(N - n)]^{1/2}$, where N is the total number (18) of rate constants, and n is the total number of parameters (6) derived from the calculations, that is, the three pairs of activation parameters corresponding to the three constants k_{-co}, k_{-c}, and k_{+c}/k_{+co}. This is found to be ±11%, which is excellent considering that the calculations include all of the uncertainties induced by variations of temperature, [CO], monitoring techniques, and wavelengths or wavenumbers.

An alternative method of solving for the unknown rate constants is to take account of the fact that the values of k_{+co}/k_{+c} are smaller at lower temperatures where the plots of k_{obs}

(21) The importance of incorporating temperature dependence data into the analysis lies in the fact that, in solving the complete set of data at all temperatures according to eq 8, there are only four unknowns, that is, the two pairs of $\Delta H^{\ddagger}$ and $\Delta S^{\ddagger}$ parameters corresponding to the two unknown rate constants at each temperature.

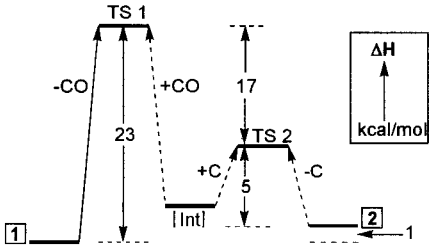

Figure 9. Enthalpy profile for reaction **1** ⇌ **2** (not drawn exactly to scale).

versus [CO] are less curved. The values of the initial slopes at low [CO], and the deviations from linearity at higher [CO], provide initial values for $k_{-c}(k_{+co}/k_{+c})$ and k_{+co}/k_{+c}. These, together with values of k_{-co}, are then used in a weighted least-squares fit to eq 8 to provide improved values of $k_{-c}(k_{+co}/k_{+c})$ and (k_{+co}/k_{+c}). These are then fitted to Eyring plots, and the calculated values of the two parameters are reinserted in eq 8 to find a yet more improved set, and this iteration can be repeated if necessary. The values of k_{+co}/k_{+c} obtained in this way are not so precise because they are obtained from the quite small curvature of the k_{obs} versus [CO] plots, particularly at lower temperatures. This contrasts with the method used above where the success of analyzing for k_{+co}/k_{+c} results from the sensitivity of eq 9 to the correct choice of k_{-c}. The values of $k_{-c}(k_{+co}/k_{+c})$ from the initial slopes lead to the corresponding approximate values of the activation enthalpies and entropies given in Table 2, and the parameters obtained by this method are clearly less precise than those obtained above. However, the two different approaches lead to essentially identical results.

The activation parameters in Table 2 allow enthalpy and entropy profiles to be drawn as in Figures 9 and 10. As is always the case in such systems, the position of the intermediate on the enthalpy profile is not known although **Int** must lie below the transition state for formation of the bridging bond, because a negative enthalpy of activation for this process can be ruled out. On the other hand, there is less of a restriction on the position of **Int** on the entropy profile because entropy changes can be positive or negative. However, the combined effects of the enthalpy and entropy positions of **Int** must be such that the free energy of **Int** lies above that of **2** to an extent that prevents it from being observed in equilibrium with **2** under an inert atmosphere.

The small positive value of ΔH° for the reaction **1** → **2** shows that the newly established C−Rh bridge bonding must be of comparable strength to the Rh−CO bond that it replaces. The actual strength of the C−Rh bond itself must be even stronger because some increase of enthalpy must accompany the distortion of the $P(NC_4H_4)_3$ ligand that occurs when the bridge is formed. The negative entropy change of −8 cal K^{-1} mol^{-1} is, however, quite unfavorable considering that the standard entropy of the CO released into the solution is ∼+40 cal K^{-1} mol^{-1}.[22]

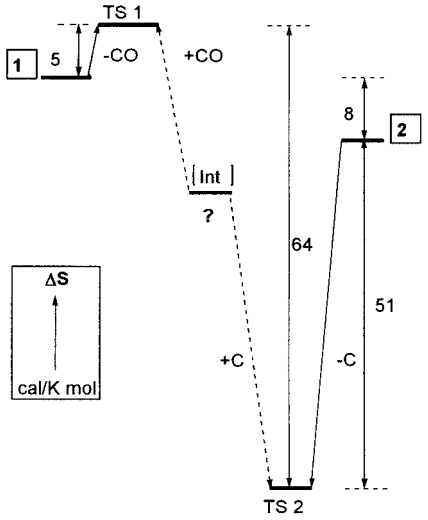

Figure 10. Entropy profile for reaction **1** ⇌ **2** (not drawn exactly to scale).

The bridged cluster therefore has a very low intrinsic entropy, that is, ∼50 cal K^{-1} mol^{-1} less than that of the $Rh_6(CO)_{15}P(NC_4H_4)_3$, the entropy of which is not expected to be out of the ordinary. This low entropy is a distinguishing feature of this unique cluster because it allows for the reversal of bridge formation, despite the enthalpic strength of the bridge bonding, something that is not observed in other bridging systems. It may be a reflection of the rather restrictive contortions that the ligand undergoes in forming the bridge.

The values of $\Delta H_{-co}^{\ddagger}$ and $\Delta S_{-co}^{\ddagger}$ are not exceptional for dissociation of a CO ligand from a metal carbonyl cluster.[23] The rather small positive entropy of activation is not at all uncommon, even negative values being obtained in some cases. These have been ascribed to the compensating occurrence of bond making that occurs within the cluster (by formation of CO bridges or by other means) and that accompanies loss of the CO ligand.[23]

Overall activation parameters can be derived from the temperature dependence of the combination of rate constants, $k_{-c}(k_{+co}/k_{+c})$, obtained from the linear dependence of the rate constants on [CO] at low values of [CO]. These correspond effectively to the second-order reaction of CO with **2** that occurs at sufficiently low values of [CO] that the highest point on the *free energy* profile for the reverse reaction is the attack of CO on **Int**. The value of 22 kcal mol^{-1} for $\Delta H^{\ddagger}$ is a bit higher than those found for the rather rare examples of bimolecular attack by CO on other carbonyl clusters,[24] but this may be ascribed to the complete breaking of the Rh−C bond in **2** before the transition state is reached. On the other hand, the positive value of +13 cal K^{-1} mol^{-1} for $\Delta S^{\ddagger}$ is very unusual for the addition of a CO ligand[24] and is another sign of the replacement of a very low entropy species (i.e., **2**) by one that is more normal (i.e., the transition state for loss of CO from **1**).

The values of $\Delta H_{-c}^{\ddagger}$ and $\Delta S_{-c}^{\ddagger}$ again reflect the major and unusual role played by entropy factors in determining the rates of reaction. Despite the considerable enthalpic strength of the C−Rh bond, $\Delta H_{-c}^{\ddagger}$ for transformation of **2** into **Int** is quite

(22) (a) The standard entropy of CO in the gas phase at 1 atm of pressure is 47.3 cal K^{-1} mol^{-1} (*National Bureau of Standards Tables of Chemical Thermodynamic Properties*; National Bureau of Standards: Washington, DC, 1982), and this can be converted to 41.1 cal K^{-1} mol^{-1} for a standard state of 1 M. These gas-phase data are likely to be applicable also to toluene solution in view of the negligible heat of solution of CO in Decalin (Basato, M.; Fawcett, J. P.; Poë, A. J. *J. Chem. Soc., Dalton Trans.* **1974**, 1350) and the conclusions of Hoff et al. (Gonzales, A. A.; Zhang, K.; Nolan, S. P.; de la Vaga, R. L.; Mukerjee, S. L.; Hoff, C. D.; Kubas, G. J. *Organometallics* **1988**, *7*, 2429) that heats of solvation of CO, H_2, N_2, and a number of liquid ligands are negligible as compared with experimental errors in calorimetric measurements.

(23) Malik, S. K.; Poë, A. J. *Inorg. Chem.* **1979**, *18*, 1241. Chen, L.; Poë, A. J. *Can. J. Chem.* **1989**, *67*, 1924. Hudson, R. H. E.; Poë, A. J. *Inorg. Chim. Acta* **1997**, *259*, 257. Poë, A. J.; Moreno, C. *Organometallics* **1999**, *18*, 5378.

(24) Poë, A. J.; Sampson, C. N.; Smith, R. T.; Zheng, Y. *J. Am. Chem. Soc.* **1993**, *115*, 3174 and references therein.

small, showing that bond strength changes are relatively minor. This suggests that the extent of bond breaking is small or that bond breaking is accompanied by largely compensating bond making. The value of $\Delta S_{-c}^{\ddagger}$, however, shows that **TS2** has a pronouncedly lower intrinsic entropy than $Rh_6(CO)_{14}(\mu\text{-}P(N_4H_4)_3)$, itself already an "improbable" species.[25] The values of $\Delta H_{+co}^{\ddagger} - \Delta H_{+c}^{\ddagger}$ ($\sim$17 kcal mol^{-1}) and $\Delta S_{+co}^{\ddagger} - \Delta S_{+c}^{\ddagger}$ (+64 cal K^{-1} mol^{-1}) in Table 2 are a measure of the enthalpic and entropic differences between **TS1 a**nd **TS2** and throw some light on the nature of **Int**. Although it is reactive, by definition, it is not all that reactive because $\Delta H_{+co}^{\ddagger}$ must be greater than 17 kcal mol^{-1} by the amount that $\Delta H_{+c}^{\ddagger}$ exceeds 0 kcal mol^{-1}. This means that formation of the new Rh−CO bond is quite difficult and that **Int** cannot have a simple vacant coordination site. The position of **Int** on the entropy profile is more difficult to estimate and depends on how much entropy gain there is on going from **TS(2)** to **Int** as compared with that on going from **Int** to **TS(1)**, that is, on how "entropically normal" **Int** is. If **Int** were a normal coordinatively unsaturated species, its intrinsic entropy, plus the entropy of the free CO, would actually be higher than that of **TS(1)**. That would make the further changes on forming **TS(2)** unfavorable by over 50 cal K^{-1} mol^{-1}, and this seems highly unlikely. It appears, therefore, that **Int** is enthalpically quite stable but is, as well, another "low-entropy" species.

(25) In an attempt to show that **TS2** is not quite such an unusual species, a value of only −20 cal K^{-1} mol^{-1} was forced on $\Delta S_{-c}^{\ddagger}$. This raised its intrinsic entropy to −33 cal K^{-1} mol^{-1} and increased $\Delta H_{-c}^{\ddagger}$ to 15 kcal mol^{-1} without changing the other parameters (particularly $\Delta H°$ and $\Delta S°$) appreciably. It did, however, increase $\sigma(k_{obs})$ to ±22%, much of which was made up of systematically lower values of k_{calc}.

What can also be said is that **Int** is not at all like the intermediate proposed above to be involved in the interchange of C(134) and C(131). This is enthalpically over 10 kcal mol^{-1} more difficult to reach than **TS2** (Table 2), and its formation is also entropically neutral in sharp contrast to formation of **TS2**. We therefore propose that **Int** might be an isomer of **2** that involves one of the other types of bonding found between aromatic rings and metal centers.[1−3] Of these, orthometalation[1] might require too much enthalpy, and formation of η^2-(C═C)[2a−e] and η^6-(C_6)[2f−i] bonds would require rotation to form the same sort of sideways-on bonded intermediates that scrambling involves. We therefore tentatively favor an agostic η^2-(C−H) intermediate[3] which would not require appreciable rotation of the ring, but which can, by virtue of the common occurrence of such species, be assumed to have quite strong bonding. While we cannot explain the large decrease in entropy that occurs, we can only conclude that the atomic movements involved are so precisely defined that this is the outcome.

Acknowledgment. Thanks are given to the Natural Science and Engineering Research Council, Ottawa, for support of this work, and to the North Atlantic Treaty Organization for a Collaborative Research Grant No. OUTR. CRG 951482.

Supporting Information Available: Details of experimental procedures, tables of rate constants, and figures showing time-dependent spectroscopic changes and exponential fitting of rate data (PDF). This material is available free of charge via the Internet at http://pubs.acs.org.

JA012440B